NASA Technical Memorandum 82677

Laser-Velocimeter Flow-Field Measurements of an Advanced Turboprop

J. S. Serafini
Lewis Research Center
Cleveland, Ohio

and

J. P. Sullivan
Purdue University
West Lafayette, Indiana

and

H. E. Neumann
Lewis Research Center
Cleveland, Ohio

Prepared for the
Seventeenth Joint Propulsion Conference
cosponsored by the AIAA, SAE, and ASME
Colorado Springs, Colorado, July 27-29, 1981

NASA

Trade names or manufacturer's names are used in this report for identification only. This usage does not constitue an official endorsement, either expressed or implied, by the National Aeronautics and Space Administration.

LASER-VELOCIMETER FLOW-FIELD MEASUREMENTS OF AN ADVANCED TURBOPROP

by

J. S. Serafini*
J. P. Sullivan**

and

H. E. Neumann*

Summary

Non-intrusive measurements of velocity about a spinner-propeller-nacelle configuration at a Mach number of 0.8 have been performed. A laser velocimeter, specifically developed for these measurements in the NASA Lewis 8- by 6-foot Supersonic Wind Tunnel, was used to measure the flow-field of the advanced swept SR-3 propeller. The laser velocimeter uses an argon ion laser and a 2-color optics system to allow simultaneous measurements of 2-components of velocity. The axisymmetric nature of the propeller-nacelle flow-field permits two separate 2-dimensional measurements to be combined into 3-dimensional velocity data. Presented are data ahead of and behind the propeller blades and also a limited set in between the blades. Aspects of the observed flow-field such as the tip vortex are discussed.

- -

* Aerospace Engineer, NASA Lewis Research Center, Cleveland, Ohio

** Associate Professor, Department of Aeronautical and Astronautical Engineering, Purdue University, West Lafayette, Indiana

around 0.8 to 0.85. The 24.5 inch diameter SR-3 propeller has eight blades with 45 degrees of sweep at the tip. For all the data presented herein, the blade angle, measured at 3/4 propeller radius ($\beta_{3/4}$), was set at 60.5°, the wind tunnel Mach number was 0.8 and the corrected propeller rotational speed was 143 revolutions per second. This yielded the design advance ratio, J, of 3.06 and power coefficient, of 1.8. For additional details on the SR-3 propeller performance and geometrical characteristics see References 5 and 6.

Laser Velocimeter System. A block diagram of the overall LV (laser velocimeter) system is shown in Figure 2. Depicted are the major system components. Before going into detail on the system components, Figure 3 is given to provide a simplified description of the principle of measurement of velocity by the fringe-type laser velocimeter. In Figure 3(a) is given the schematic of a typical fringe-type LV for a single color. After exiting the laser the beam is split by a beam splitter into two parallel beams which are then focused by a lens system to cross at a given point in space. Figure 3(b) depicts the nature of the intersection of the beams. Since the two beams each consist of coherent planar wavefronts (of the same wave-length), the intersection region, commonly referred to as the probe volume, contains parallel interference fringes which have a

$$\text{fringe-spacing} = \frac{\lambda}{2 \sin(\theta/2)}$$

where λ is the wave-length and θ is the included angle between the two intersecting beams.

As a very small(of the order of 1 micron) seed particle with velocity, V_z, crosses fringes, the radiation scattered from the seed particle is measured by a photomultiplier sensing equipment and the frequency and/or inverse period resulting is

$$\text{Frequency} = \frac{1}{\tau} = \frac{2V_z}{\lambda}\sin(\theta/2)$$

where τ is the period.

A more detailed and sophisticated treatment of laser velocimeters including the fringe-type LV is given in Reference 18.

The major components of the LV system are shown in Figures 4 thru 6. The components shown in Figure 4 are all essentially depicted by the block labelled "LASER AND OPTICS" in Figure 2. The Spectra-physics Model 171-8 Argon Ion Laser has strong lines at

wavelengths of 488.0 nm (blue) and 514.5 nm (green). Also seen in Figure 4 is the four beam, two color TSI Inc. optics system which was modified for use in this particular configuration. The two color beam exiting from the laser is color separated using a dispersion prism which results in clear color separation with a minimum of crosstalk between the beams. Also seen in Figure 4 is the portion of the optics which includes the beam-splitting and adjusting sections. For this set of experiments the four beams were set up such that the planes defined by the two beams of each color were nominally orthogonal to each other and at nominally 45° to the horizontal plane of the wind-tunnel reference system. This portion also includes the on-axis receiving optics including the two photomultiplier tubes.

The four beams exiting the TSI Inc. optics then pass through a zoom lens system (specially designed and made by Pacific Optical). The function of the zoom lens is, to vary the location of the probe volume from 3 to 12 feet which provides the ability to survey across the wind tunnel. The back-scattered radiation from the seed particles in the probe volume was received through the 9-inch output lens of the zoom lens system and entered the TSI optics where it ultimately was sensed by the two photomultiplier tubes, one for the 488.0 nm blue signal and one for the 514.5 nm green signal. These signals were amplified by the TSI combined power-supply and amplifier unit and then were fed through coaxial cables to the measuring and monitoring instrumentation located remotely from the wind-tunnel test section in the control room (see Figure 6).

Probe Volume Movement. As indicated above the position of the beam cross-over or probe volume was varied laterally (perpendicular to the wind-tunnel side-wall) by means of the zoom lens system. Vertical and horizontal displacement occurred by mechanically moving the optical bed-plate mounted on the traversing table (see Figure 5). All three DC motors, one for the movable lens on the zoom and the two for the traversing table, are driven by digital motor controllers which in turn are controlled by a microcomputer. The microcomputer sequences all the positioning functions. The microcomputer also checks position limits to prevent overtravel and times all functions to assure that the positioning motors are responding to commands.

Remote Control and Instrumentation. The amplified blue and green signals from the photomultiplier tubes are fed into the Macrodyne Two-channel LV Processor, Model 2098 (Figure 6)which operates on the counter principles (as a result of the number and timing of the crossing of a seed particle). This processor has multiple validation criteria, the most important one being the 5 to 8 count comparison. This check will eliminate the data being taken with two or more particles in the probe volume at the same time. This processor has the capability of processing signals up to 100 MHz

frequency and a 1 MHz data rate capability. Adjustable high-pass and low-pass filters are available to maximize the signal/noise ratio of the signals. The output from the processor, given as the inverse of the frequency, is available in digital and analoque forms. For purposes of on-line monitoring, the analogue signals along with the unprocessed signals were fed into spectrum analyzers, oscilloscopes and data-rate counters. The digital signal from the processor was fed via an interface unit into the minicomputer for further processing. For each blue and green inverse frequencies (periods) handled by the minicomputer a propeller position was acquired by the minicomputer. The propeller position was generated by using the once-per-revolution signal generated by a magnetic pick-up on the propeller shaft along with a shaft angle encoder made by Real Time Systems Inc., Model 371.

The DEC 11/34 Minicomputer was programmed to control the positioning of the measurement point or probe volume in the three directions as previously described. It interacted with the LV processor and shaft angle encoder to accept data points consisting of digital words giving the blue and green periods (1/frequency) and propeller position. The number of data points accepted can be as high as 4000. The acquired data can be selectively stored on disk or shown on a on-line graphics output (with hard copy available). A summary of the data was always listed on-line as printer output. Available plots on the graphics output used were (1) the periods as a function of propeller position and (2) a histogram of the inverse/periods for the accepted data.

Seeding of Wind-tunnel. Many attempts were made to seed the wind-tunnel using various types of seeding materials, various methods of particle formation and particle dispersion into the wind-tunnel. The final version of the seeding system used for the investigation reported herein incorporated the use of two units of TSI Inc., Model 9306, Six Jet Atomizer. The seeding fluid was Di Octyl Phthalate (DOP). The recommended air flow rate of 12 liters/minute was used. The atomizers are air driven at 55 psig. Increasing the seed flow-rate beyond that specified tended to cause agglomeration of the seed particles. The seed particles were introduced into the plenum of the wind-tunnel just upstream of the flow-straightening tubes and screen. This position is 60 feet upstream of the turboprop model spinner. The seed was generated outside the tunnel and flowed through 27 feet of pipe (1-inch diameter). The end of the pipe was open and pointed downstream. Four such pipes were placed either in vertical or horizontal arrays with the pipe separations being 12 to 15 inches apart. This arrangement of the seed pipes provided the seed cloud required for either the vertical surveys or the horizontal surveys through the model centerline. Data supplied with the TSI Inc. Six Jet Atomizer indicated that, using DOP, the particle size distribution was such that 75% were less than 1 micron and 98% were less than 2.0 microns at the atomizer discharge. Measurements of the particle lag near

the hub of the spinner and the oscilloscope signals of the particles crossing the fringes (Fig. 3) were consistent with the TSI specifications. Within the middle of the seeding cloud, the measured data rates varied from 500 to 1000 per second in the free-stream to 50 to 100 per second behind the blades. When measurements were taken in the periphery of the seeding clouds, the data rates dropped to values lower than 50.

Experimental Procedure. Prior to each wind-tunnel run, the propeller blade angle was set. The seed pipes in the plenum were arranged in the desired vertical or horizontal array. To obtain radial (referenced to the model centerline) and axial velocity components from the two color LV optics, the seed pipes were arranged vertically along a line through the model centerline. To obtain the azimuthal and axial velocity components, the seed pipes were arranged horizontally along a line through the model centerline.

The alignment of the optics was checked to assure that the two blue beams and two green beams were crossing properly at their focus to insure that good, bright and parallel fringes existed. As earlier remarked, these blue and green fringes were nominally orthogonal to each other and nominally 45° to the horizontal plane. Next, by using a low-speed, seeded 1-inch diameter air-jet, the quality of the Doppler signal was checked both at the test-section and also remotely in the control room. Finally, these signals were fed through the LV processor and into the minicomputer for further evaluation of the "state-of-readiness" of the LV optics. After the readiness of the optical of the system was verified, the operation of the zoom lens and transversing table were checked-out through the minicomputer. The positions of all four beams relative to the wind-tunnel reference frame were measured and calibrated. From this information the beam angles and probe volume positions were later calculated. Then, the position of the spinner tip (and other parts of the model, as required) were noted in terms of the zoom lens and traversing table read-outs.

Figure 5 shows the acoustically-treated environmental enclosure which was mechanically isolated from the the optical bed-plate. Adjacent to the viewing window, the enclosure had a hole sufficiently-sized to permit the laser beams to exit the enclosure. Cooling water lines were connected to the enclosure. When proper operating conditions of the wind-tunnel and turboprop model were achieved, usually Mach 0.8 and either wind-milling condition or an advanced ratio, J, of 3.06 for the turboprop model the laser was remotely turned on and brought up to a beam power of 2 to 4 watts. Next the seeders were turned on. The TV monitors were available to give indications of the laser beams in the seed cloud and the general condition of turboprop model and the LV system next to the test section. The probe volume was positioned via the computer terminal. The LV signals were checked by monitoring the oscilloscopes, spectrum analyzers and data-rate monitors and the data-taking process commenced using terminal instructions to the minicomputer.

Data Analysis. The on-line outputs included earlier-mentioned minicomputer terminal print-outs and the hard copy from the graphics terminal, (Fig. 6). The terminal print-out contained the probe volume position information, LV processor information, number of data points recorded and the time the data was taken. For both blue and green channels the mean and r.m.s. periods (1/frequency) and frequency were given. Also given was whether or not all the raw data points were stored on disk. A software program was generated to permit the calculation of velocity components in the Cartesian coordinates in the wind-tunnel reference frame. For a given probe volume position, the acquired data over a complete revolution of the propeller (360^{0} of azimuthal coordinate relative to the once-per-revolution pulse) is divided into 80 "angular" bins per 360^{0} or 240 "angular" bins per 360^{0}. The averaged velocities in these "angular" bins were calculated. For the data analyzed and presented herein, the data for the 8 blades over 360^{0} has been folded into and averaged over 0^{0} to 45^{0} relative to the once-per-rev pulse. Also calculated were the time-averaged velocities for each probe volume position.

Operating Problems. Initially, the major problems of concern were the vibrations due to the wind-tunnel compressor and the increase in temperature in the air about the laser and optics during transonic operation (up to 140^{0}F). Although the LV system did not operate during supersonic operation of the wind-tunnel, it was still necessary to provide cooling protection for the LV laser and optics to prevent possible misalignment and damage. The initial design to meet the vibration problem islated the traversing table from the wind tunnel structure. The temperature problem was handled by embedding water cooling coils on the surface of a box covering the LV laser and optics.

First attempts at transonic operation revealed a problem not previously anticipated. As the Mach number increased to 0.8 and 0.85, the laser beam power dropped off to near zero and could not be brought into control. From discussions with the manufacturer's staff, it was discovered that the laser becomes "detuned" as the ambient pressure decreases significantly. Since it was not feasible to set-up the laser at the reduced pressure levels encountered at transonic operation, the problem was solved by enclosing the laser in a pressure-tight enclosure with a quartz window at one end and keeping the enclosed space at atmospheric pressure.
Problems with vibration and intense acoustic levels still interfered with maintaining alignment of the LV optics. So the tunnel air-blast coming through the "transonic bleed" holes was shielded from hitting the enclosure over the LV optics and laser by an air-blast shield seen in Figure 5. To better isolate the LV laser and optics, vibration isolation devices were inserted between the optics bedplate and the traversing table and complete direct mechanical separation between the two was maintained. To reduce the ambient acoustic pressure level of 155 db in the test

chamber to permissible values, the environmental enclousre was revamped using acoustical treatment material (Fig. 5) in addition to the cooling coils embedded in the surface. Also, cooling of the optical bedplate was installed to minimize warping of the bedplate surface due to temperature variations.

Results and Discussion

The results presented herein comprise a part of a complete set of data taken to enable a mapping of the flow field for the SR-3 propeller operating at the design point of $\beta_{3/4} = 60.5^{o}$, Mach = 0.8, advance ratio, J = 3.06 and power coefficient, Cp = 1.8. Not presented at all herein are a set of wind-milling data which, along with the powered data, permits the calculation of the radial blade loading (Ref. 17). The data are in the wind-tunnel reference frame and are given in terms of a cylindrical coordinate system. It is centered along the turboprop model centerline with positive z in the downstream direction referenced to the spinner tip. The angular coordinate is measured clockwise facing downstream (direction of propeller rotation) and $\phi = 0^{o}$ for a radius pointing upward vertically.

Several typical examples of the type of raw data acquired are given in Figure 7 which presents the period in nanoseconds (output from the LV processor) as a function of the shaft angle encoder output for the green signal. This data, consisting of 1000 points, is from the hard-copy available from the on-line graphics. This data was acquired with the probe volume positioned at a radial distance, r/R = 0.76, where the propeller radius, R = 12.25 inches. For Figure 7(a), the probe volume is at z/R = 0.49 and the azimuthal angle, $\phi = 90^{o}$). At this radial position the probe volume is just ahead of the leading edge of the blade. The upstream influence of the blade can be seen. Figure 7(b) is an example of the type of raw data obtained with the probe volume positioned "in between" the blades (z/R = 0.74 and $\phi = 90^{o}$). There is some evidence of blade "flash" as the blades intersect the probe volume. It is particularly heavy for the first and fourth blades in Figure 7(b). The blade "flash" occurs are as a result of the blade surface back-scattering into the probe volume a suficient amount such that it appears as a "pseudo-particle" as far as the LV system is concerned. Figure 7(c) is for a probe volume position downstream of the trailing edge (z/R = 0.98 and $\phi = 180^{o}$). Evidence of the wakes of the 8 blades is seen as the 8 vertical stacks of points in the plot (the larger the period, the slower the velocity). Because the probe volume diameter (diameter = 0.035 inches and the length = 0.35 inches) is not much smaller than the blade wake thickness a good resolution of the wake profile may not be possible. In addition to the evidence of the wake, Figure 7(d) (z/R = 0.81 and $\phi = 180^{o}$) shows an example of the shadowing by the blades that occurred over a portion of the survey region at $\phi = 180^{o}$.

Figure 8 gives a cross-section of the SR-3 propeller, spinner and nacelle. The coordinates are given as r/R, radial distance and z/R, axial distance, where R = 12.25 inches. The SR-3 blade is shown in the sketch such that it is at the measured $\beta_{3/4}$ and the $\Delta\beta$ or twist of the blade is also accounted for. Thus, the SR-3 blade in the sketch is correctly represented at a $\phi = 0^{o}$ (vertical upward position) as viewed by the LV system beams. Also, specified in Figure 8 are two upstream stations, A and B and two downstream stations, C and D, at which radial measurements (z/R = constant) are presented in later figures.

In Figure 9 are given the time-averaged (and circumferentially averaged) components of velocity, V_z, V_ϕ and V_r as a function of r/R at constant values of z/R. Figure 9(a) presents the axial component, V_z, as a function of r/R for Station A (z/R = 0.09), Station B (z/R = 0.33), Station C (z/R = 0.89) and Station D (z/R = 1.14). The velocity, V_z, data of Figure 9(a) shows the trends expected for a spinner-propeller-nacelle configuration. At Station A for small values of r/R the velocity V_z is suppressed considerably as a result of being near spinner the tip (z/R = 0.09) and increases to near free-stream values of velocity at large values of r/R. At Station B the velocity V_z behaves similarly. At Station C and D, the velocities V_z at values of r/R = 1.0 or less are higher than at Station B, as expected, because of work done by the propeller on the airstream as it moves through the blades. Figure 9(b) gives the time-averaged azimuthal velocity, V_ϕ, as a function of r/R for Station A through D. At Station A and B, ahead of the blades, the values of V_ϕ were quite small and at Station C and D, behind the blades, the values of V_ϕ increased considerably for r/R = 1.0 or less, as expected. Using values of V_z from Figure 9(a) and V_ϕ from Figure 9(b) the measured swirl angles can be calculated from

$$\text{swirl angle,} \qquad \varepsilon = \tan^{-1} \left(V_\phi / V_z\right)$$

then at r/R = 0.75, (3/4 radius), at Station C

$$\varepsilon = \tan^{-1} (72.5/825) = 5.0^{o}$$

and at Station D and r/R = 0.75

$$\varepsilon = \tan^{-1} (45/890) = 2.9^{o}$$

The time-averaged radial velocity, V_r, is given in Figure 9(c) for Station A through D. The behavior for all the four stations as r/R increases is similar and decrease from values of 150 to 175 feet/sec as r/R increases to values around 25 to 30 feet/sec. This behavior is consistent with the presence of the spinner-nacelle.

Figure 10 presents a typical example of the velocity data acquired with the probe volume position being in between the blades (r/R = 0.76, z/R = 0.74, see Figure 8) and ϕ of the probe

volume position = 90°). The data for the 8 blades has been "folded over" so that the 30 angular bins (each bin = 1.5°) cover an angular displacement of 45°. Figuire 10(a) presents the axial velocity, V_z, as a function of the azimuthal angle, ϕ. As noted earlier, $\phi = 0°$ is referenced to the once per rev signal. In going from 0° to 12.75° the "pressure" or underside of the blade is approached. At $\phi = 17.25°$ and greater the field adjacent to "suction" or upper surface of the blade is being measured and, of course, the data at 45° is continued by going back to 0° on the plot. In Figure 10(a) the data points at ϕ = 14.25° and 15.75° are not valid velocity points because of the aforementioned blade "flash" effect (and also blade thickness). Otherwise, the data in Figure 10(a) appears to be well-behaved. The unfolded data, not presented herein in the interest of brevity, does show a measure of blade-to-blade differences in the flow-field which is to be expected. Figure 10(b) gives the azimuthal velocity, V_ϕ, as a function of ϕ. Again, the blade "flash" points are noted. Also occurrring is an abrupt change in V_ϕ across the blade of about 60 feet/sec.

Figure 11 gives a comparison of the velocities measured at a radial position just inboard of the blade tip with those just outboard of the blade tip. With the probe volume at $\phi = 90°$ and z/R = 0.89 (Station C just downstream of the trailing edge of the blade tip), the "just inboard" radial position is at r/R = 0.98 and the "just outboard" radial station is at r/R = 1.02. Figure 11(a) gives the axial velocity V_z as a function of the azimuthal angle, ϕ, for both values of r/R. Fig. 11(b) gives the azimuthal velocity, V_ϕ, as a function of ϕ for both values of r/R. Fig. 11(b) clearly shows the effect of the tip vortex. The peaks in the velocity V are of opposite signs comparing the r/R = 0.98 data with the r/R = 1.02 data. It should be noted here that V_ϕ is positive for clockwise rotation looking downstream (also, clockwise rotation of propeller). Therefore, the negative V_ϕ at r/R = 1.02 gives the tip vortex the correct rotation (from the lower surface to the upper surface at tip of blade). Now, by looking at the V_z velocity in Fig. 11(a) at r/R = 1.02, outboard of the blade tip, there is seen a sharp drop in velocity with the decrease in velocity being about 250 feet/sec. This is also taken to be a distinctive effect of the tip vortex of the blade. The V_z velocity data given in Fig. 11(a) for r/R = 0.98 appears to have some similarities with the in-between blade data of Fig. 10(a) in that for values of ϕ less than 24°, with the flow coming from the "pressure' side of the blade, the V_z velocities are less than those at ϕ greater than 24° with the flow coming from the suction side of the blade. Because of the relatively thin blade wake near the tip, none of the data points give any evidence of the wake. The jump in V_z velocity at r/R = 0.98 in Fig. 11(a) should also be partly the result of the mesurement position being slightly inboard of the tip vortex of the blade.

The final figure, Figure 12, illustrates another aspect of the tip vortex by providing data on a set of axial traverse points at a constant r/R. The data in Figure 12 is for constant r/R = 1.08 at a probe volume $\phi = 180^{\circ}$ and with taking various z/R from 0.80 to 1.28. The value of r/R = 1.08 is further outboard than that for Figure 11 (r/R = 1.02). A value of z/R = 0.80 corresponds to an axial position just downstream of the leading edge at the tip (see Figure 8) and z = 1.28 is downstream of Station 0. In Figure 12(a), the axial velocity, V_z, is given as a function of the azimuthal angle, ϕ. Looking at the set of data reveals that as this r/R = 1.08 survey point moves downstream the angle at which the vortex is felt (dip in the V_z velocity) increases. Also, the magnitude of the dip in V_z increases as the survey station, z/R moves downstream. Both these effects are consistent with the previously presented picture of the tip vortex and its screw-like trajectory downstream of the propeller.

Figure 12(b) presents the radial velocity, V_r, as a function of azimuthal angle, ϕ (remembering that the probe volume $\phi = 180^{\circ}$, here). The data in Figure 12(b) is also for r/R = 1.08 and z/R survey points from 0.80 to 1.28. Here, again, the results beg a similar interpretation for the radial velocity, V_r, behavior in Figure 12(b) as for the V_z velocity behavior in Figure 12(a). There is, in addition, an asymmetry of the V_r velocities about $V_r = 0$, but this was expected from the data on the time-averaged V_r data presented in Figure 9(c). A particularly good picture of the tip vortex is seen for the z/R = 1.28 survey point as ϕ goes from $\phi = 7^{\circ}$ to about $\phi = 13^{\circ}$.

Concluding Remarks

A laser velocimeter system has been successfully developed to obtain velocity measurements in the hostile environment associated with the transonic operation of the NASA Lewis 8- by 6- foot Supersonic Wind Tunnel. Particularly severe environmental problems such as high levels of vibration and noise were overcome by successful designs and redesign of the LV system. The laser velocimeter used an argon ion laser and a two-color optics system which yielded two components of velocity simultaneously. By taking advantage of the axisymmetric nature of the propeller-nacelle flow-field the two-dimensional measurements on the vertical and horizontal radii were combined into three-dimensional velocity data. The LV system has obtained a set of flow-field measurements, a part of which are presented herein to demonstrate the data quality and to present and discuss certain characteristics of the flow-field ahead of, within and behind the blades. This data was taken at a Mach number of 0.8 and the propeller at an advance ratio of 3.06 with a blade angle setting at three-fourths radius of 60.5°. This data should be useful for extending the understanding of advanced propeller flow fields and for verifying the emerging propeller analysis codes.

References

1. Rohrbach, C. and Metzger, F. B., "The Prop-Fan - a New Look in Propulsors," AIAA Paper 75-1208, Sept. 1975.

2. Mikkelson, D. C. Blaha, B. J., Mitchell, G. A., and Wikete, J. E., "Design and Performance of Energy Efficient Propellers for Mach 0.8 Cruise," NASA TM X-73612, 1977.

3. Bober, L. J. and Mitchell, G. A., "Summary of Advanced Methods for Predicting High Speed Propeller Performance," NASA TM 81409, 1980.

4. Rohrback, C., "A Report on the Aerodynamic Design and Wind Tunnel Test of a Prop-Fan Model," AIAA Paper 76-667, July 1976.

5. Jeracki, R. J., Mikkelson, D. C., and Blaha, B. J., "Wind Tunnel Performance of Four Energy Efficient Propellers Designed for Mach 0.8 Cruise," NASA TM 79124, 1979.

6. Jeracki, R. J. and Mitchell, G. A., "Low and High Speed Propellers for General Aviation - Performance Potential and Recent Wind Tunnel Test Results," NSA TM 81745, 1981.

7. Sullivan, J. P., "The Effect of Blade Sweep on Propeller Performance," AIAA Paper 77-716, June 1977.

8. Young, W. H., Meyers, J. E., and Hoad, D. R., "A Laser Velocimeter Flow Survey Above a Stalled Wing,"AVCROM TR-78-50, NASA TP-1266, 1978.

9. Johnson, D. A., Bachalo, W. D., and Modarress, D., "Laser Velocimeter Supersonic and Transonic Wind Tunnel Studies," Proceedings of the Minnesota Symposium on Laser Anemometry, E.R.G. Eckert, ed., University of Minnesota, Minneapolis, MN, 1976, pp. 68-82.

10 Sullivan, J. P., Widnall, S. E., and Ezekiel, S., "Study of Vortex Rings Using a Laser Doppler Velocimeter," AIAA Journal, Vol. 11, No. 10, Oct. 1973, pp. 1384-1389.

11. Seasholtz, R. G., "Laser Doppler Velocimeter System for Turbine Stator Cascade Studies and Analysis of Statistical Biasing Errors," NASA TN D-8297, 1977.

12. Goldman, L. J., Seasholtz, R. G., and McLallin, K. L., "Velocity Surveys in a Turbine Stator Annular-Cascade Facility Using Laser Doppler Techniques," NASA TN D-8269, 1976.

13. Powell, J. A., Strazisar, A. J., and Seasholtz, R. G., "Efficient Laser Anemometer for Intra-Rotor Flow Mapping in Turbo-Machinery," ASME Journal of Engineering for Power, Vol. 103, No. 2, Apr. 1981, pp. 424-429.

14. Strazisar, A. J. and Powell, J. A., "Laser Anemometer Measurements in a Transonic Axial Flow Compressor Rotor," ASME Journal of Engineering for Power, Vol. 103,No. 2, Apr. 1981, pp. 430-437.

15. Landgrebe, A. J. and Johnson, B. V., "Measurement of Model Helicopter Rotor Flow Velocities with a Laser Doppler Velocimeter," Journal of the American Helicopter Society, Vol. 19, No. 3, July 1974, pp. 39-43.

16. Biggers, J. C., Lee, A., Orloff, K. L., and Lemmer, O. J., "Measurements of Helicopter Rotor Tip Vortices," American Helicopter Society Preprint AHS 77-33-06, May 1977.

17. Sullivan, J. P., "LDV Measurements on Propellers," Laser Velocimetry and Particle Sizing, Proceedings of the Third International Workshop, H. D. Thompson and W. H. Stevenson, eds., Hemisphere Publishing Corp., Washington, DC, 1979, pp. 531-534.

18. Durst, F., Melling, A., and Whitelaw, J. H., Principles and Practice of Laser-Doppler Anemometry, Academic Press, Inc., London, 1976.

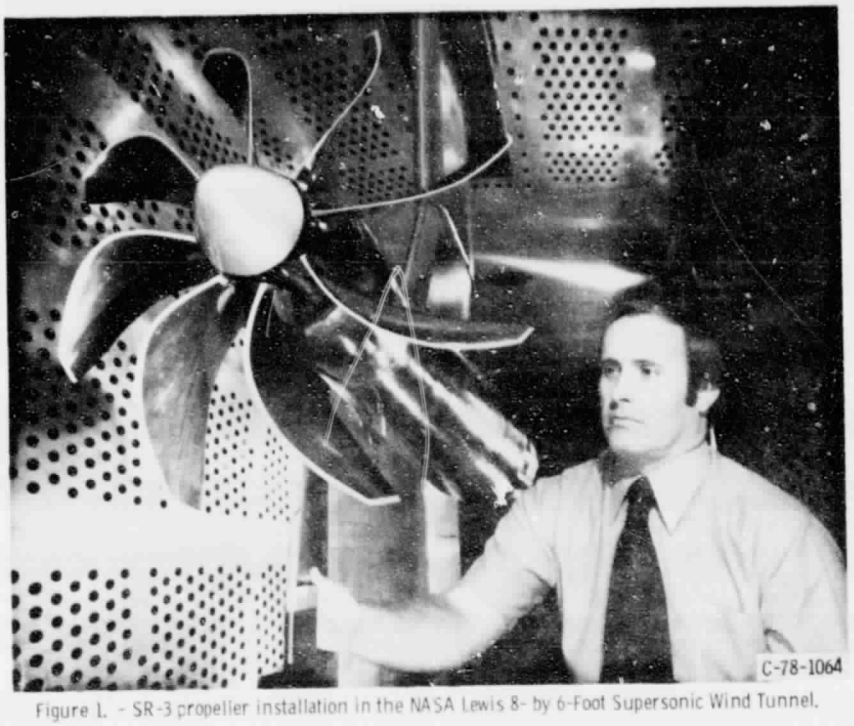

Figure 1. - SR-3 propeller installation in the NASA Lewis 8- by 6-Foot Supersonic Wind Tunnel.

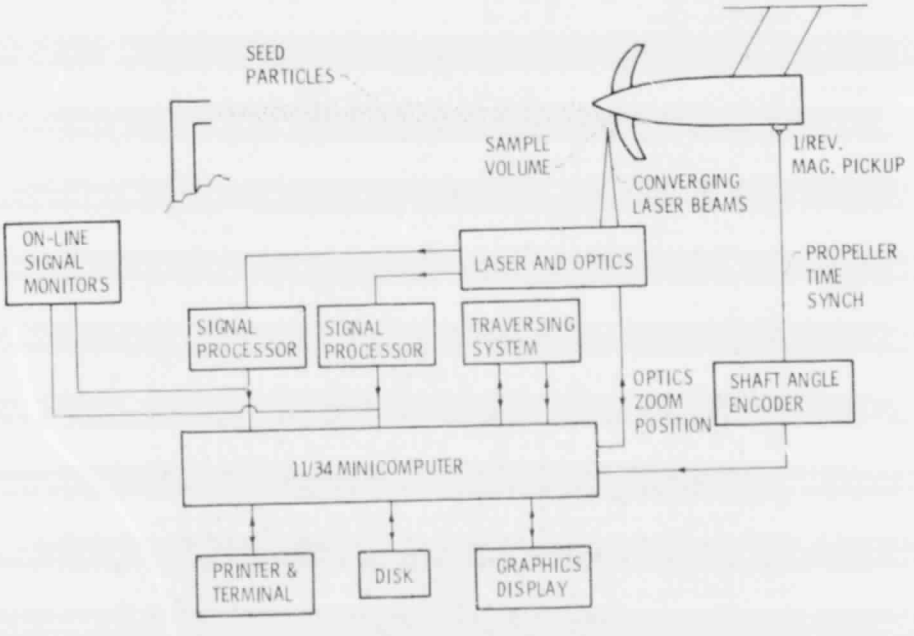

Figure 2. - Block diagram of the laser velocimeter system.

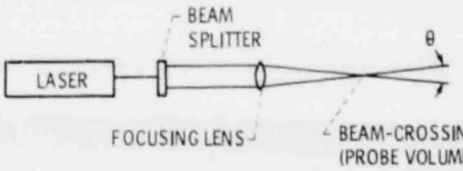

(a) Schematic of dual-beam laser velocimeter for one color.

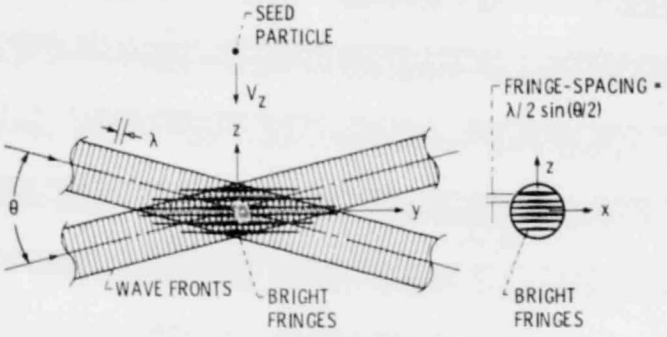

FREQ = $1/\tau = (2V_z/\lambda) \sin \theta/2$

(b) Enlarged schematic of probe volume.

Figure 3. - Sketch of the fringe-mode laser velocimeter.

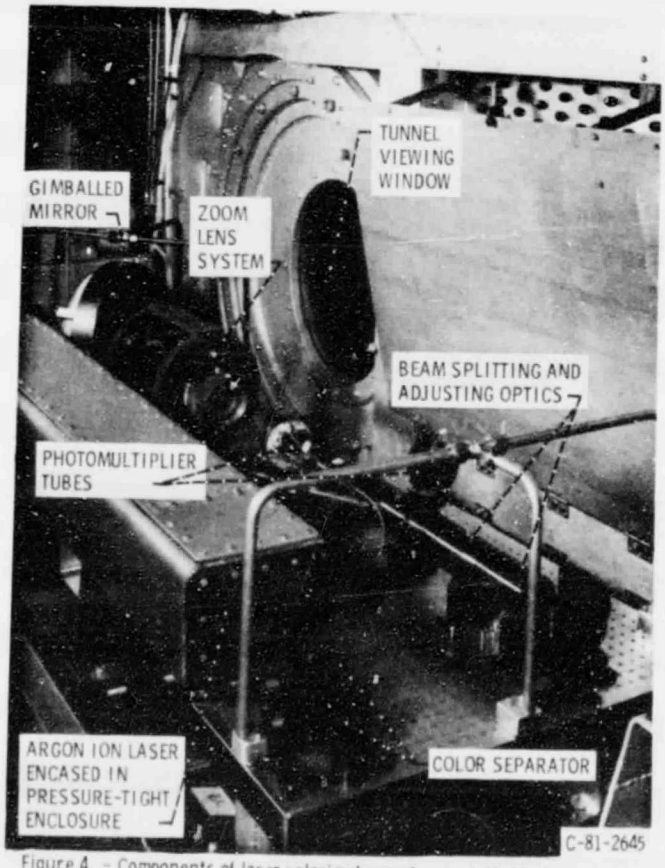

Figure 4. - Components of laser velocimeter system installed in 8- by 6-Foot NASA Lewis Supersonic Wind Tunnel.

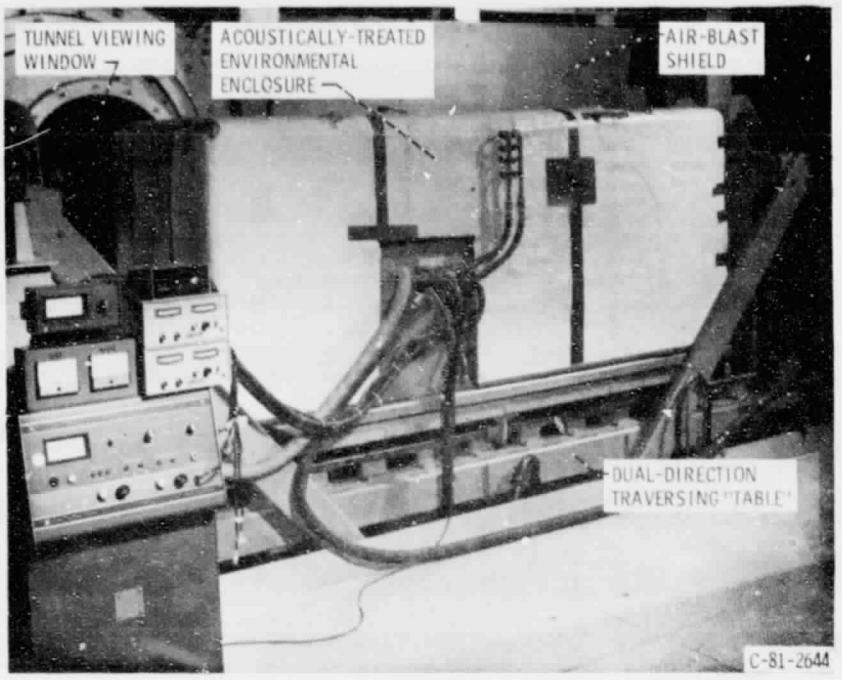

Figure 5. - Laser velocimeter system components covered with the environmental enclosure.

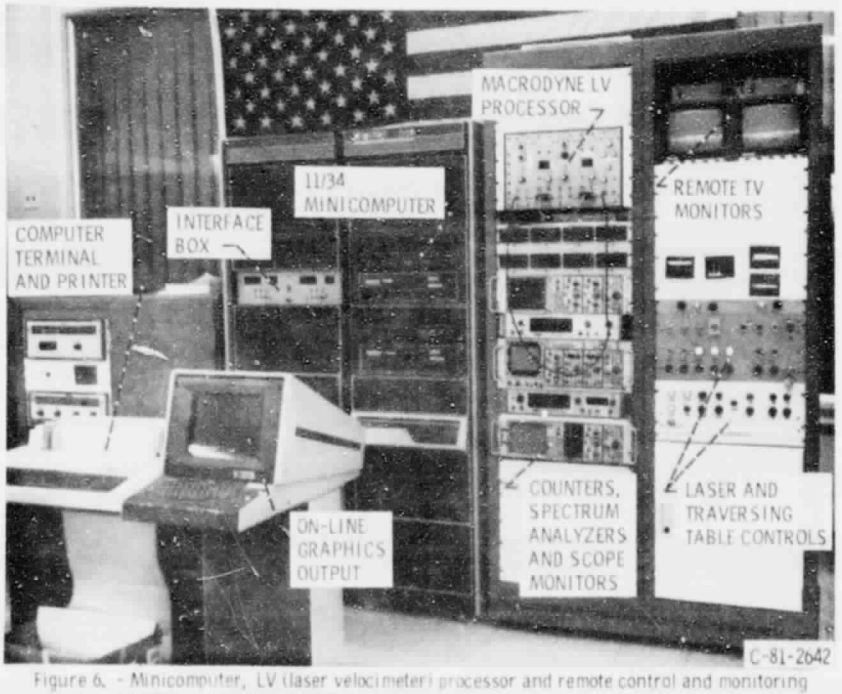

Figure 6. - Minicomputer, LV (laser velocimeter) processor and remote control and monitoring instrumentation of the LV system.

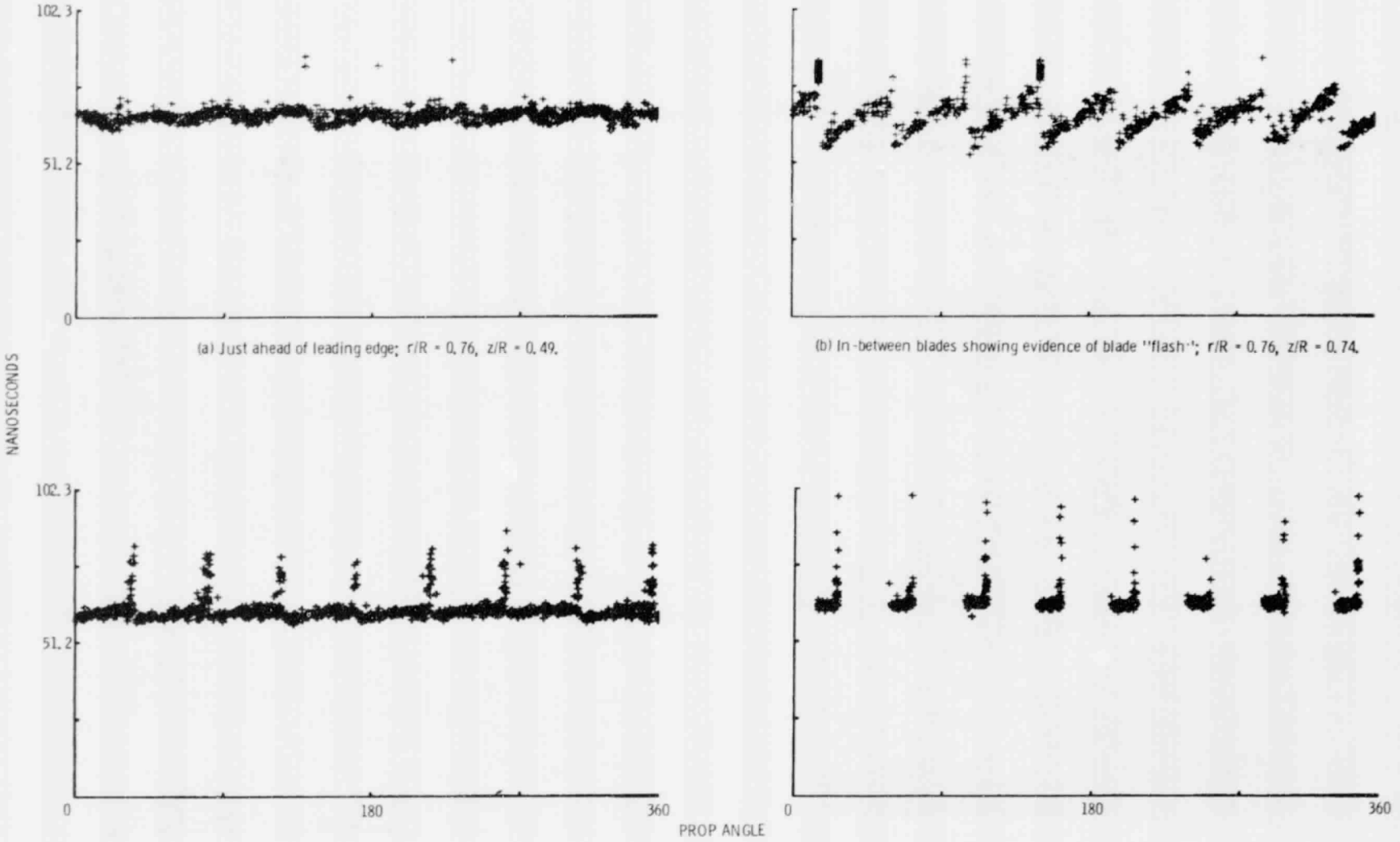

(a) Just ahead of leading edge; r/R = 0.76, z/R = 0.49.

(b) In-between blades showing evidence of blade "flash"; r/R = 0.76, z/R = 0.74.

(c) Behind trailing edge showing evidence of wake; r/R = 0.76, z/R = 0.98.

(d) Behind trailing edge showing evidence of blade shadowing and wake; r/R = 0.76, z/R = 0.81.

Figure 7. - Typical examples of the on-line data that could be displayed graphically and stored on disks.

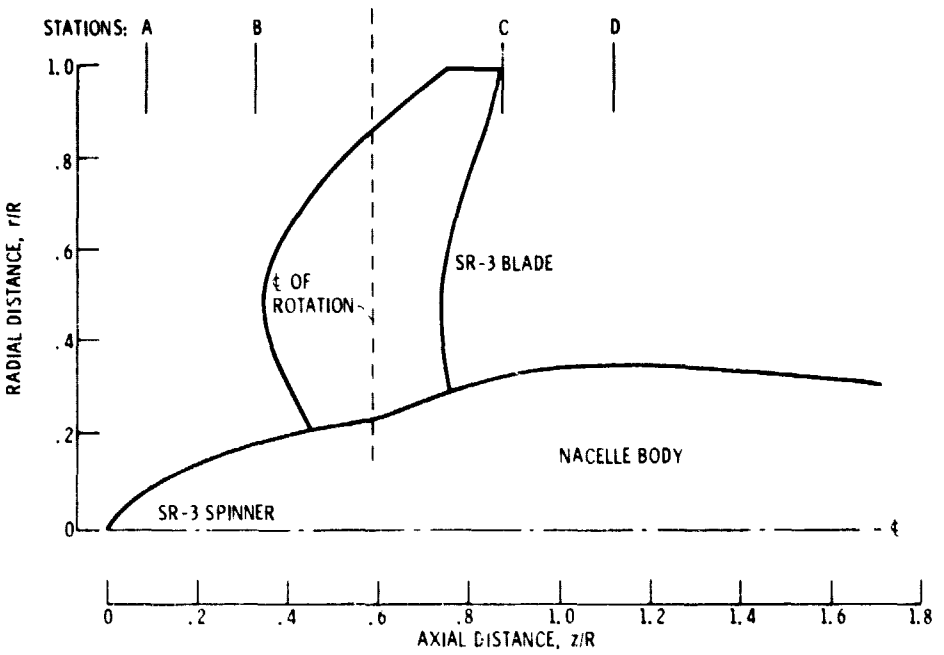

Figure 8. - Sketch of SR-3 propeller, spinner, and nacelle.

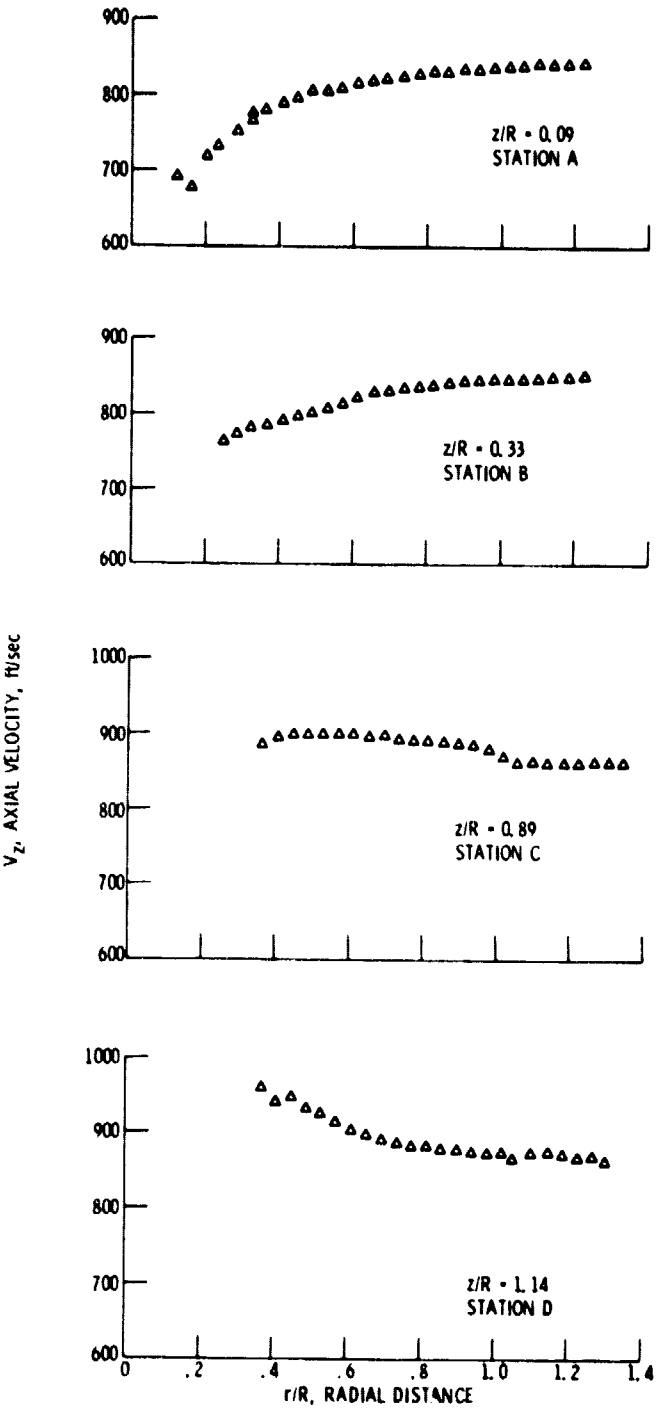

(a) Axial velocity, V_z, as a function of r/R.

Figure 9. - Time-averaged (and circumferentially averaged) velocity as a function of radial distance, r/R.

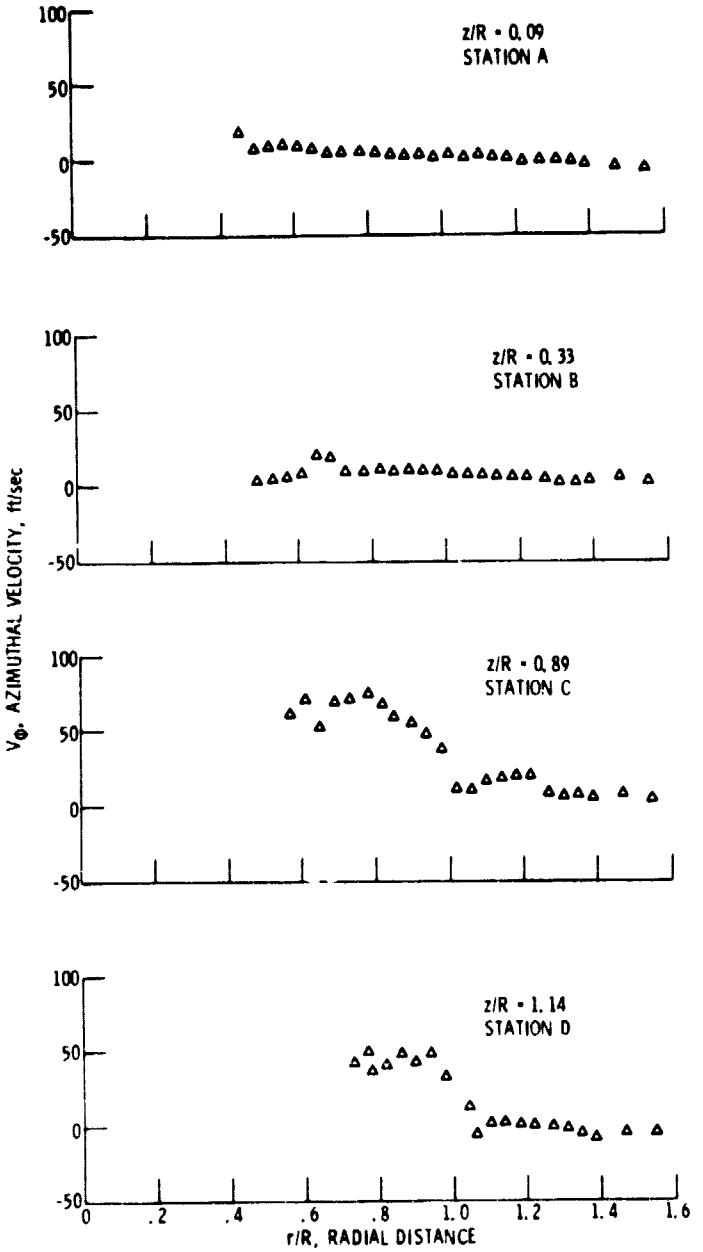

(b) Azimuthal velocity, V_ϕ, as a function of r/R.

Figure 9. - Continued.

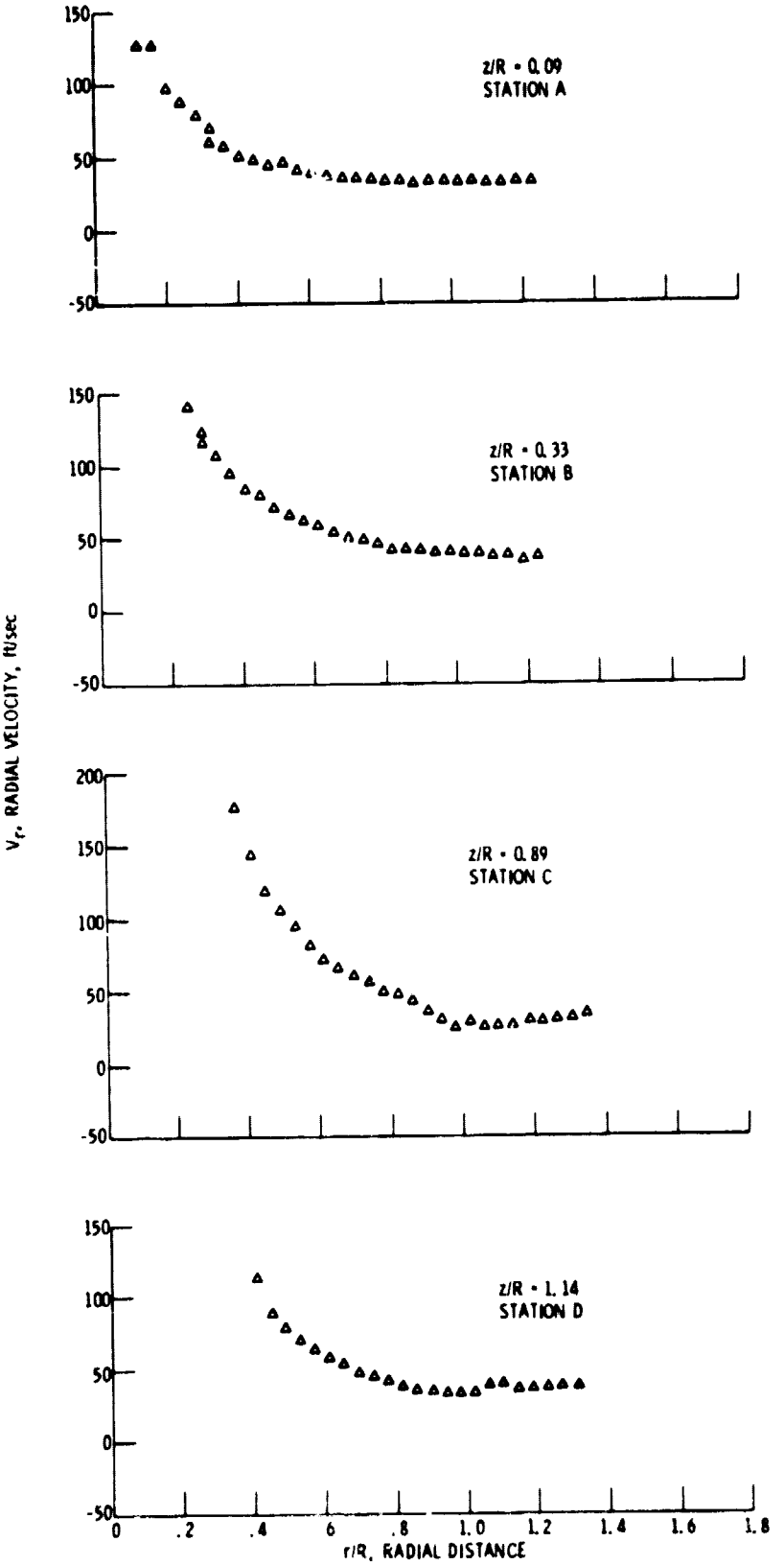

(c) Radial velocity, V_r, as a function of r/R.

Figure 9. - Concluded.

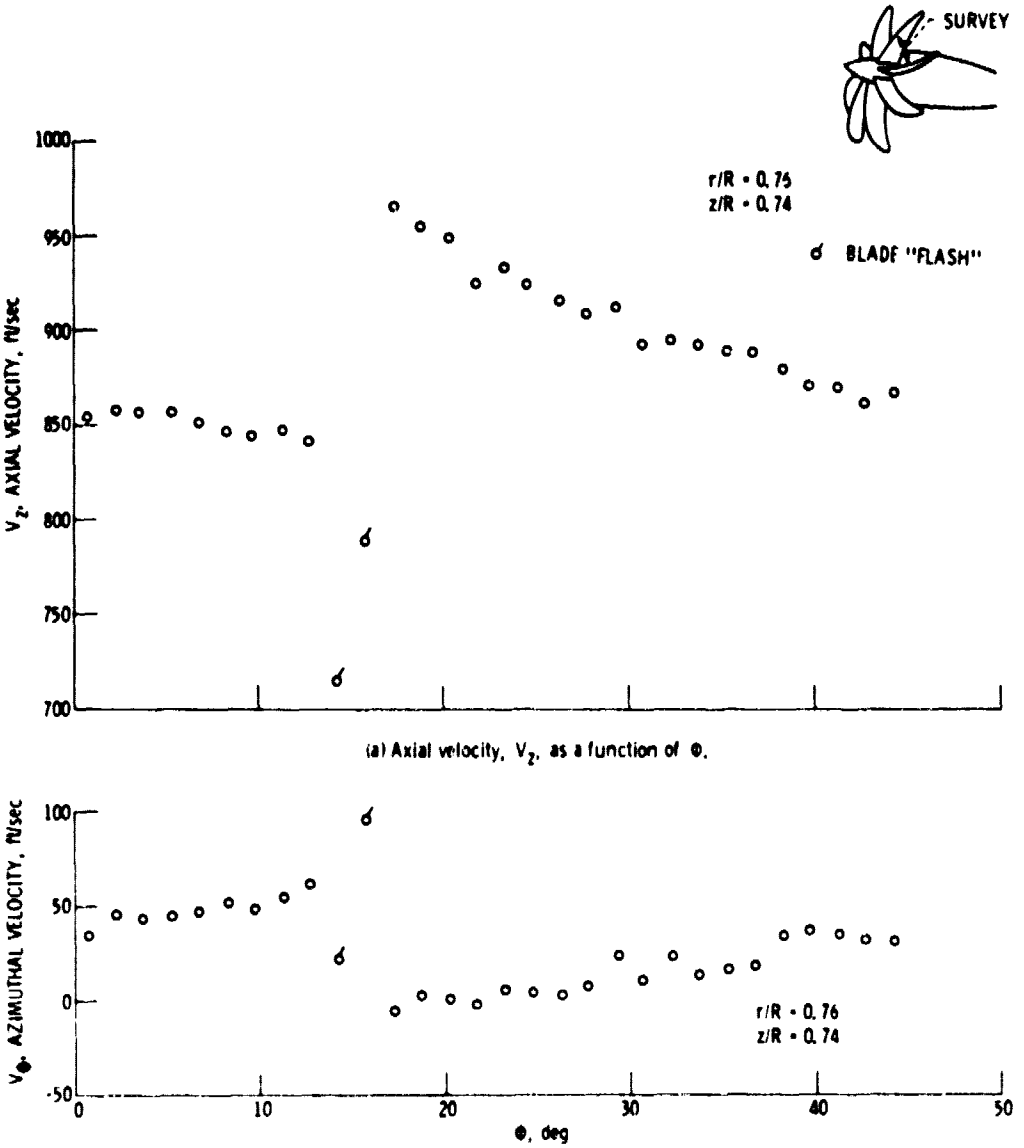

(a) Axial velocity, V_z, as a function of Φ.

(b) Azimuthal velocity, V_Φ, as a function of Φ.

Figure 10. - Typical data acquired between the prop blades.

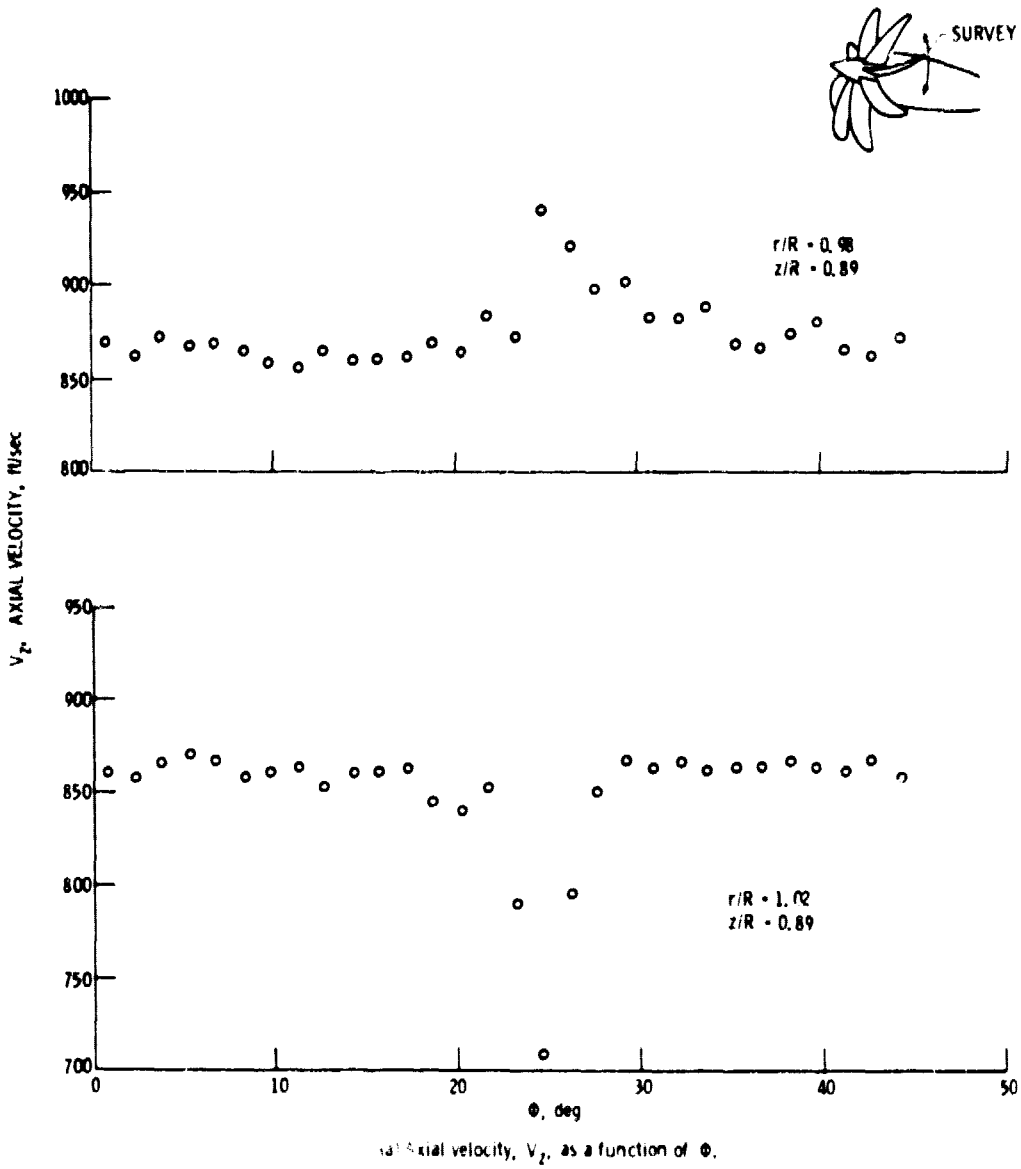

(a) Axial velocity, V_z, as a function of Φ.

Figure 11. - Comparison of velocities measured at radial positions just inboard of tip with those just outboard of tip, station C.

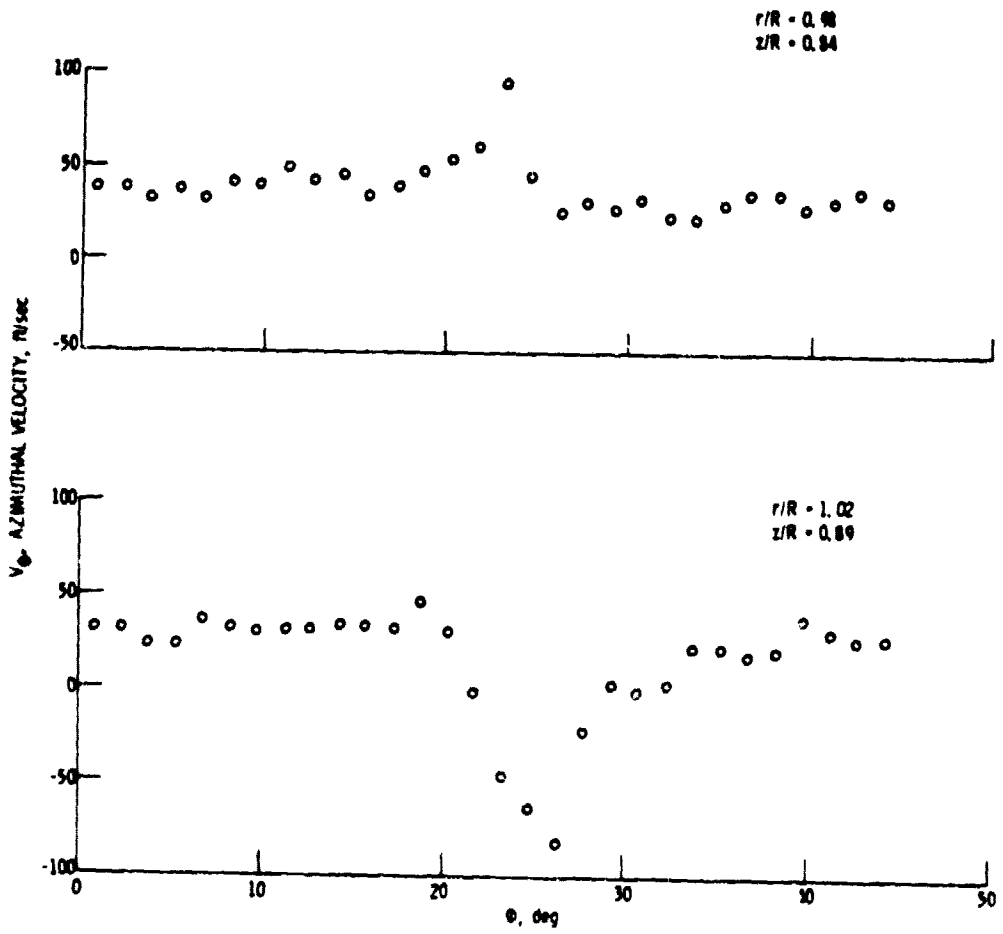

(b) Azimuthal velocity, V_Φ, as a function of Φ.

Figure 11. - Concluded.

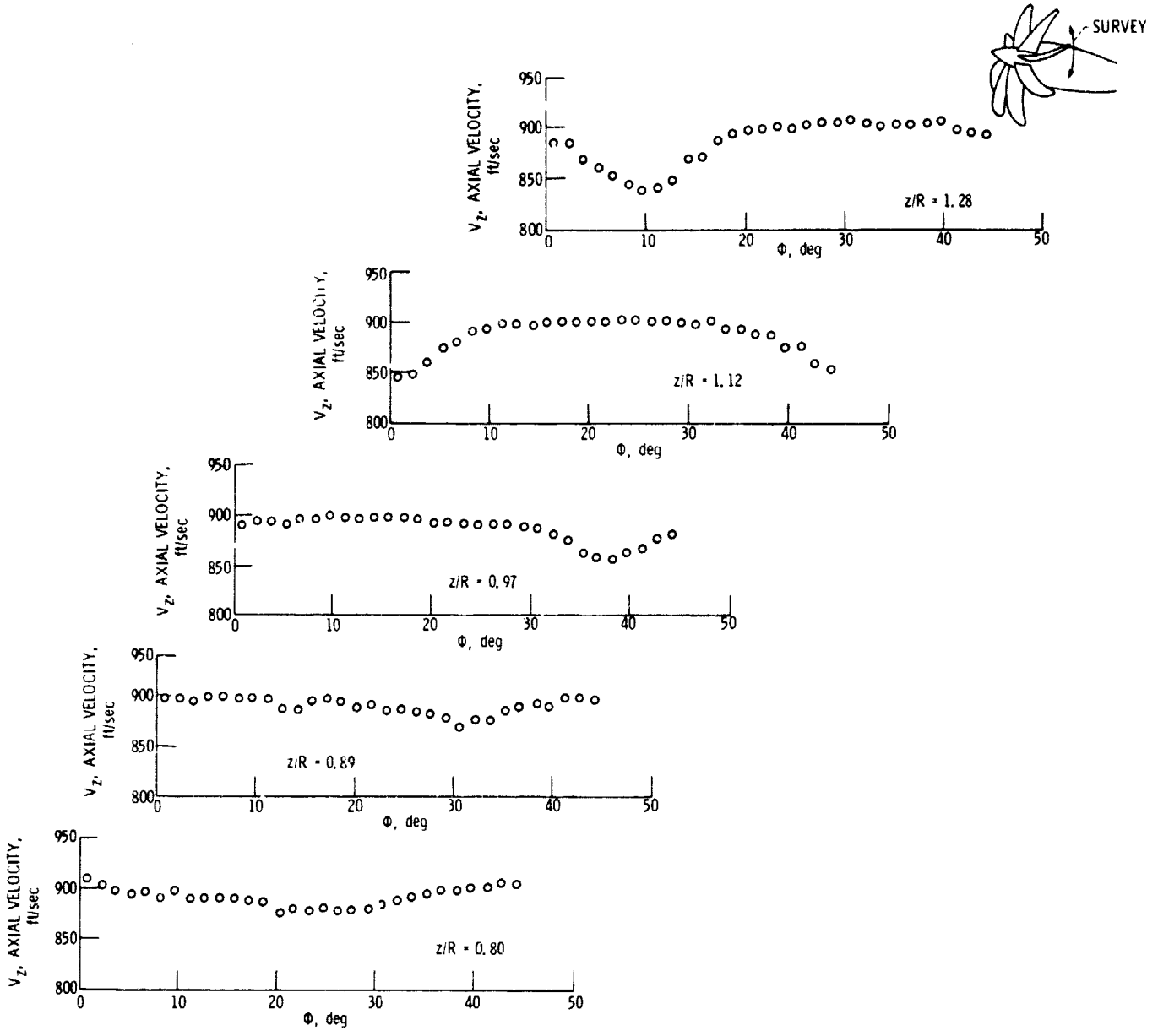

(a) Axial velocity, V_z, as a function of Φ.

Figure 12. - Comparison of velocities measured at various axial distances at a r/R of 1.08.

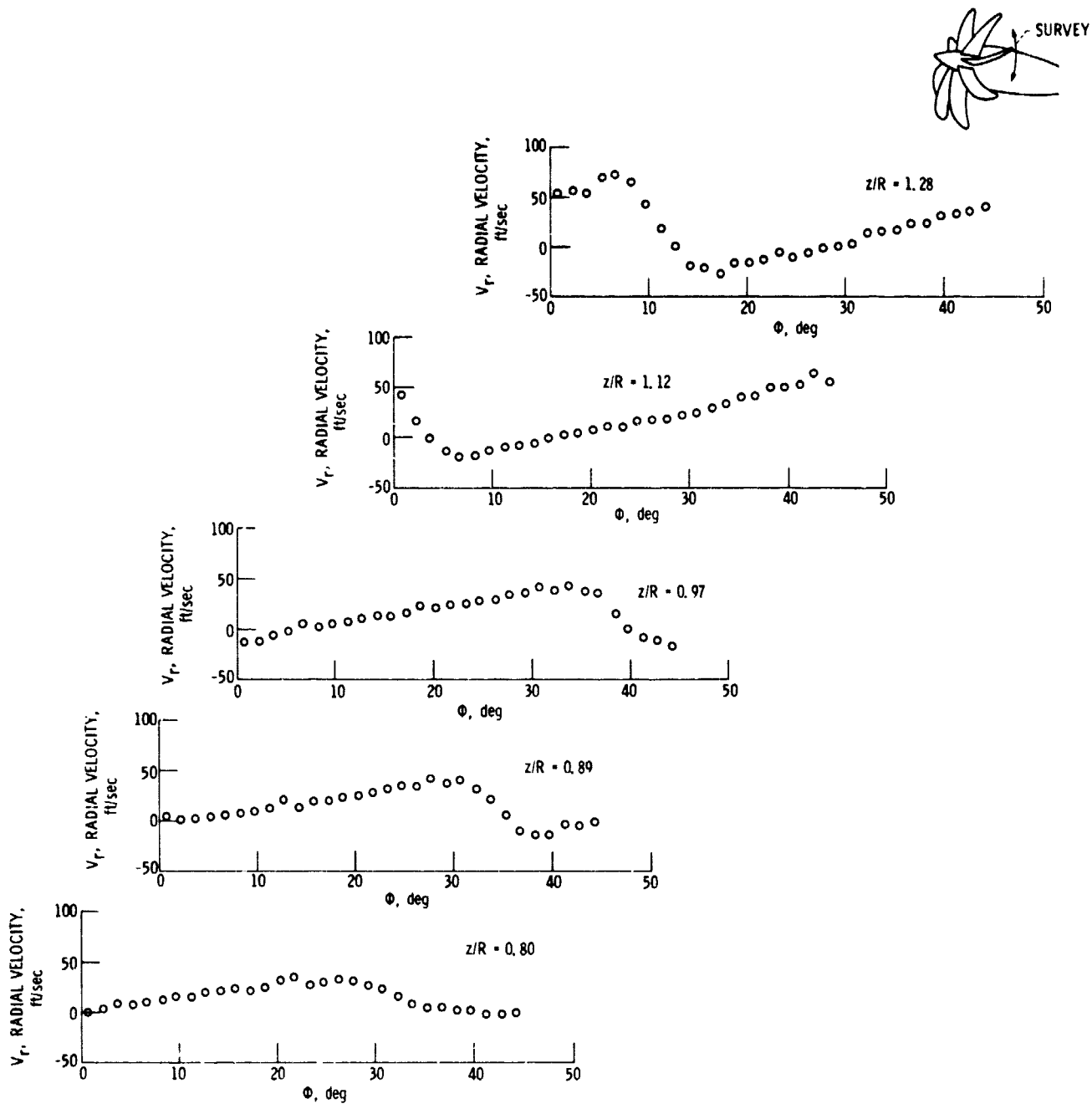

(b) Radial velocity, V_r, as a function of Φ.

Figure 12. - Concluded.